Submitted to Ap.J.
Preprint typeset using LaTeX style emulateapj v. 11/10/09

HELIUM SHELL DETONATIONS ON LOW MASS WHITE DWARFS AS A POSSIBLE EXPLANATION FOR SN 2005E

Roni Waldman[1], Daniel Sauer[2], Eli Livne[1], Hagai Perets[3], Ami Glasner [1], Paolo Mazzali [4 5 6], James W. Truran [7 8], Avishay Gal-Yam [9]

Submitted to Ap.J.

ABSTRACT

Recently several type Ib supernovae (SNe; with the prototypical SN 2005E) have been shown to have atypical properties. These SNe are faint (absolute peak magnitude of ~ -15) and fast SNe that show unique composition. They are inferred to have low ejecta mass (a few tenths of a solar mass) and to be highly enriched in calcium, but poor in silicon elements and nickel. These SNe were therefore suggested to belong to a new class of calcium-rich faint SNe explosions. Their properties were proposed to be the result of helium detonations that may occur on helium accreting white dwarfs. In this paper we theoretically study the scenario of helium detonations, and focus on the results of detonations in accreted helium layers on low mass carbon-oxygen (CO) cores. We present new results from one dimensional simulations of such explosions, including their light curves and spectra. We find that when the density of the helium layer is low enough the helium detonation produces large amounts of intermediate elements, such as calcium and titanium, together with a large amount of unburnt helium. Our results suggest that the properties of calcium-rich faint SNe could indeed be consistent with the helium-detonation scenario on small CO cores. Above a certain density (larger CO cores) the detonation leaves mainly ^{56}Ni and unburnt helium, and the predicted spectrum will unlikely fit the unique features of this class of SNe. Finally, none of our studied models reproduces the bright, fast evolving light curves of another type of peculiar SNe suggested to originate in helium detonations (SNe 1885A, 1939B and 2002bj).

Subject headings: nucleosynthesis, hydrodynamics, supernovae

1. INTRODUCTION

Recently, a new type of peculiar type Ib supernova (SN) has been discovered (with the prototypical SN 2005E and a full sample of 8 SNe; Perets et al. 2010a). These helium rich SNe show several intriguing features. They show fast and faint light curves (B-band peak luminosity of -15) and dominant lines of calcium in the nebular spectrum. Only a small fraction of radioactive nickel is found in their ejecta, and Si group elements seem to be completely absent in their nebular spectra. In addition, the environment of these SNe is typically old (Perets et al. 2010a,b); inconsistent with massive young progenitors, usually thought to be associated with type Ib SNe. It was therefore proposed that these objects may result from helium detonations that occur on helium accreting white dwarfs. Energetically, the moderate observed velocities of $11,000$ km sec^{-1} together with the estimated ejected mass (a few tenths of a solar mass), are consistent with the binding energy of $0.2\,M_{\odot}$ of helium.

Other peculiar low mass and even faster evolving SNe, but bright (peak luminosity of ~ -18.5) have also been studied (de Vaucouleurs & Corwin 1985; Chevalier & Plait 1988; Poznanski et al. 2010; Perets et al. 2010c). These SNe have also been suggested to result from helium detonations. Although we shall remark on these SNe, their light curves are brighter and faster than those produced in our simulations, and are unlikely to be produced by these scenarios.

In the past decades, several authors discussed the scenario of detonations in helium layers, accreted on carbon-oxygen cores, suggesting "peculiar" SNe with faint, fast light curves (see e.g. Woosley et al. 1980; Nomoto 1980, 1982; Woosley et al. 1986; Livne 1990; Livne & Glasner 1990, 1991; Woosley & Weaver 1994; Livne & Arnett 1995). There are several main issues here which deserve close investigation. The first issue is the explosion mechanism and especially the question whether a detonation which develops first in the helium layer could ignite a second (successive) detonation in the CO core. The second important issue includes the nucleosynthesis and its impact on the shape of both the light curve and spectrum. The third issue is the evolution of helium accreting white dwarfs to thermonuclear runaway.

The question whether a second detonation occurs has

[1] Racah Institute of Physics, The Hebrew University, Jerusalem 91904, Israel
[2] Stockholm University, Department for Astronomy, AlbaNova University Center, 106 91 Stockholm, Sweden; Current Address: Meteorological Institute, Ludwig-Maximilians-University, Theresienstr. 37, 80333 Munich, Germany
[3] Harvard-Smithsonian Center for Astrophysics, 60 Garden St., Cambridge MA, USA 02138
[4] Max-Planck Institut für Astrophysik, Karl-Schwarzschild-Str. 1, 85748 Garching, Germany
[5] Scuola Normale Superiore, Piazza dei Cavalieri 7, 56126 Pisa, Italy
[6] Istituto Naz. di Astrofisica-Oss. Astron., vicolo dellOsservatorio, 5, 35122 Padova, Italy
[7] Physics Division, Argonne National Laboratory, Argonne, IL 60439
[8] Department of Astronomy and Astrophysics, Enrico Fermi Institute, and Joint Institute for Nuclear Astrophysics, University of Chicago, 5640 South Ellis Avenue, Chicago, IL 60637
[9] Benoziyo Center for Astrophysics, Faculty of Physics, The Weizmann Institute of Science, Rehovot 76100, Israel

been discussed many times. If this happens, the process will lead to the disruption of the entire star, and the consequences will be completely different from those obtained in the case where the core is not burning. Livne & Glasner (Livne 1990; Livne & Glasner 1990, 1991) have studied this, where a small reaction network of 13 species has been used. Under the assumption of spherical symmetry, the CO core always experiences ignition at the center, after a converging pressure wave, which propagates from the core-helium boundary, reaches the center (Livne 1990; Woosley & Weaver 1994). However, in a more realistic scenario, helium detonation is unlikely to start at a spherical shell simultaneously. Rather it is more likely to ignite at a small area near the interface, which can be approximated by a point ignition. The problem becomes a two dimensional problem with cylindrical symmetry around an axis defined by the line connecting the center of the star and the ignition point. Livne & Glasner (1990, 1991) have shown two ways by which the core can be ignited in this case. Depending on actual parameters (mainly the density of the fuels near the interface), the sliding helium detonation emits a strong oblique shock into the adjacent CO core, which in some cases is strong enough to drive a CO detonation near the interface. Otherwise, converging shock waves propagate inwards and eventually converge on the axis, but in this case off center. Consequently, driving a second CO detonation from that convergence point is also probable if the density there is not too low. Note however that those results were obtained for rather massive CO cores of $0.85\,M_{\odot}$ and above.

The main study of the second important issue, namely the role of nucleosynthesis in the explosion and its appearance, has been done by Woosley & Weaver (1994), who performed a series of one dimensional simulations using a detailed reaction network. They used CO cores between $0.6\,M_{\odot}$ and $0.9\,M_{\odot}$ with helium mantles between $0.13\,M_{\odot}$ and $0.63\,M_{\odot}$ (where the total was kept below the Chandrasekhar limit). In agreement with Livne (1990), they find that the core is being ignited in all cases by converging pressure waves. A common important observable feature of those models is their very fast light curve, which rises to maximum over roughly 10-12 days. The amounts of ^{56}Ni vary among models, between $0.2\,M_{\odot}$ and $0.98\,M_{\odot}$, with strong correlation between the core mass and the amount of ^{56}Ni produced. Moreover, significant amounts of calcium and titanium isotopes are being synthesized. Interestingly, similar results were obtained by 2D simulations (Livne & Arnett 1995), where similar models were simulated under the assumption of point ignition. A more comprehensive study in both 2D and 3D was recently carried out by Fink et al. (2007). Their results confirm the main conclusions of the previous multi-dimensional studies.

Finally, the evolution of helium accreting white dwarfs to thermonuclear runaway is a very complicated subject. Moreover, the onset of helium detonation at the base of such helium layers is a speculative process, yet to be explored. Some progress has been recently reported by Shen & Bildsten (2009). In the context of our study, their main result is the minimal helium mass required for dynamical burning as function of core mass (Fig. 5 there). They also point out that the exact composition of the accreted helium plays an important role in the runaway. Previous results, published by Yoon & Langer (2004) are consistent with the above. However, they focused on the possible effects of rotation and found that rotation may inhibit the runaway.

In this paper we ignore most of the above complications and repeat the work of Woosley & Weaver (1994), but extend the range of core masses to lower values. Contrary to previous work, which focused on the higher edge of the mass range, we are interested here in low mass progenitors which presumably can reproduce the observations of SN 2005E-like objects. Note that part of the phase space of low mass cores was also recently (and independently) studied by Shen et al. (2010), as we shall briefly discuss later.

2. EXPLOSION MODELS

2.1. *Tools and initial configurations*

We use the hydro code Vulcan/1D (V1D) which consists of an explicit Lagrangian scheme. The reaction network is based upon REACLIB with 160 elements between hydrogen and Ni, including neutrons, ^{1,2}H, ^{3,4}He, ^{7}Li, ^{7}Be, ^{8}B, $^{12-14}$C, $^{13-15}$N, $^{14-18}$O, $^{17-19}$F, $^{18-22}$Ne, $^{20-23}$Na, $^{21-26}$Mg, $^{23-27}$Al, $^{24-30}$Si, $^{27-31}$P, $^{29-34}$S, $^{31-37}$Cl, $^{33-38}$Ar, $^{36-39}$K, $^{37-44}$Ca, $^{40-45}$Sc, $^{41-50}$Ti, $^{44-51}$V, $^{45-54}$Cr, $^{48-55}$Mn, $^{49-58}$Fe, $^{50-59}$Co, $^{53-64}$Ni (Weiss & Truran 1990). The initial models are hydrostatic configurations, consisting of CO cores, with masses of 0.45, 0.5 and $0.6\,M_{\odot}$, and He layers of 0.15, 0.2 and $0.3\,M_{\odot}$. The CO core consists of pure, equal mass fractions of ^{12}C and ^{16}O, while the He layer is pure ^{4}He (except for the model discussed in 2.3, which had ^{12}C mixed into the He layer). The CO core is assumed to be isentropic, with central temperature of 10^{7}K and density that fits the given core mass. The helium layer is also isentropic, with bottom temperature of 2×10^{8}K (Yoon & Langer 2004; Shen & Bildsten 2009). Our temperatures are a bit higher than those used in Woosley & Weaver (1994) and therefore our densities are slightly lower. The models are well resolved with more than 1000 spatial zones, where the CO core is represented by ≈ 500 zones, gradually growing from $0.001\,M_{\odot}$ at the center to $0.005\,M_{\odot}$ at $0.05\,M_{\odot}$ below the edge of the core, then gradually decreasing to $10^{-4}\,M_{\odot}$ and remaining at this value throughout the He layer. In Table 1 we detail the hydrostatic parameters of the cases we have simulated.

The detonation at the base of the helium layer is driven artificially by giving 20 zones large positive radial velocity of $10^{9}\,\mathrm{cm\,s^{-1}}$. Usually this drives a detonation immediately, but, at very low density the detonation may die out after a short period of time. This suggests that the question of how/when helium detonation may be ignited spontaneously, should be studied separately under appropriate conditions and smaller scales. In any case, when formed, the self sustained detonation is rather weak, leading to incomplete helium burning over most of the layer. As mentioned earlier, spherically symmetric simulations lead always to CO ignition at the center. To avoid this complication we artificially inhibit here the burning in the core. This is temporarily justified by the fact that in the 2D case the convergence of those waves is off center, and may not ignite the core when the density at the convergence region is low enough [see Livne & Glasner

(1990, 1991) for details].

The simulation is run without rezoning until the shock wave approaches the center (typically at $\simeq 0.1\,M_\odot$ from the center, $\simeq 1\,$s after the detonation is ignited, see Fig. 1). From then on, as the He layer draws away from the core, the core is rezoned more and more coarsely. This is done in order to prevent the shocks, that are going back and forth through the core, from unnecessarily diminishing the time step (this does not affect the dynamics of the He layer). The simulation is run until $10^5\,$s, at which epoch the densities in the He layer are low enough so that radiative transfer calculations can be carried out. Nuclear reactions are followed only above a temperature of $10^7\,$K, whereas weak interaction decays are followed throughout the simulation for all zones in the helium layer.

2.2. *Results*

The evolution of the density, temperature, and velocity profiles of a typical model CO.45He.2, having a CO core of $0.45\,M_\odot$ and He layer of $0.2\,M_\odot$, is shown in Fig. 1. The initial velocity of $10^9\,\mathrm{cm\,s^{-1}}$ at $t = 0$ injected at the base of the He layer (in order to initialize the detonation) can be seen. At $t = 0.1\,$s, a detonation front has already formed, the maximum temperature in the He layer is $1.8\times10^9\,$K. At $t = 1\,$s, the outward going shock has swept through all of the WD, while the inward going shock is approaching the center. The maximum temperature in the He layer at this stage is $1.5 \times 10^9\,$K, whereas in the core it reaches $2.5 \times 10^8\,$K. It is worthwhile to mention that when the shock reaches the center, the temperature there sharply rises to $\approx 1.3 \times 10^9\,$K. At $t = 10\,$s, the velocity in the He layer is nearly homologous, and nuclear burning has almost ceased, as the maximum temperature in the He layer has dropped to $1.5 \times 10^8\,$K. From then on, as can be seen for $t = 100\,$s and $t = 10^5\,$s, the He layer continues expanding homologously, nuclear reactions being exclusively weak-interaction decays.

The compositions of our models are plotted in Fig. 2. The plotted epoch is $10^5\,$s, at which point the model is transferred to the radiative transfer calculation. For each model the figure shows (left panel) the composition by elements, and (right panel) the summed up composition of the species constituting the decay chains considered in the radiative transfer calculations (see Sec. 3).

The main nucleosynthetic products from our simulations are summarized in Table 2. **The main result of our simulations is the sharp drop of radioactive nickel products for cores below** $0.6\,M_\odot$. Accordingly, larger amounts of ^{40}Ca, ^{44}Ti and ^{48}Cr are produced, with almost no silicon group elements.

In addition we note, that the remnant CO core is expected to undergo pulsations due to the inward moving shock wave initiated by the detonation being repeatedly reflected from the center and the outer boundary of the core, but this phenomenon is not adequately resolved in our present simulations.

2.3. *Effect of initial composition on nucleosynthesis*

A major drawback of pure helium detonations is the fact that usually the burning goes all the way to ^{56}Ni, and there is no evidence for intermediate mass elements in the emerging spectrum. One way to overcome this drawback, as we demonstrate here, is to ignite the detonation at low densities. Once a pure helium detonation is ignited at densities below approximately $5 \times 10^5\,\mathrm{g\,cm^{-3}}$, the burning rate is low enough so that the composition, for the appropriate dynamic timescale, includes many intermediate mass elements and almost no iron group elements (Table 2, Fig. 2).

Another possible way to generate a composition of ejecta dominated by intermediate mass elements is to ignite the detonation in a mixture of helium and carbon (or CO). For the relevant temperatures we obtain, the triple α reaction is slow compared to α capture on carbon. Therefore, any pre existing ^{12}C will tend to capture the free α particles. It follows that, if there are sufficient carbon nuclei present at the onset of burning, the end products can be calculated by a straight forward argument.

The number N of available α particles per ^{12}C is given by:

$$N = (X_{He}/4)/(X_C/12) = 3(X_{He}/X_C) \qquad (1)$$

where X_{He} and X_C are the mass fractions of ^{4}He and ^{12}C respectively.

Initially $X_C + X_{He} = 1$, therefore the number N of available α particles a ^{12}C nucleus will ultimately accumulate is $N = 3(1 - X_C)/X_C$.

We assume here that α captures simply continue up the α capture chain from ^{12}C.

In this way, for any initial pre existing carbon abundance X_C, we can compute N and predict the end product. For initial carbon abundance X_C, the predicted major final nucleus in the aftermath of the detonation is given in Table 3. Once the final nucleus is produced, there are no more free α particles available for capture on heavy nuclei or for consumption by the triple α reaction.

For a model in which we artificially assumed an initial carbon abundance of $X_C = 0.3$, there are seven free α particles for each carbon atom and indeed the end product of the detonation is found to be ^{40}Ca, in accordance with the predictions given in Table 3.

A crucial issue for such a scenario is the origin of the pre existing carbon. Assuming that the outburst occurs on a carbon WD that accretes helium, carbon enrichment can take place if there is dredge up mixing at the bottom of the envelope prior to the ignition of the detonation. Preliminary 1D models show that the helium envelope is indeed unstable to convection about a day before the runaway. We intend to examine this interesting possibility for the mixing process by performing 1D and 2D simulations of the pre runaway evolution.

3. RADIATIVE TRANSFER MODELS

To connect the theoretical predictions from the explosion models to the observed properties of SN 2005E, radiative transfer models which describe the generation and propagation of light within the ejecta are needed. Here we investigate different aspects. First we discuss models of the bolometric light curve describing the temporal evolution of the total light emission in ultraviolet, optical and infrared (UVOIR) wavelength bands. Secondly, we computed a sequence of synthetic spectra for the early epochs from the time of explosion to about a week after maximum light.

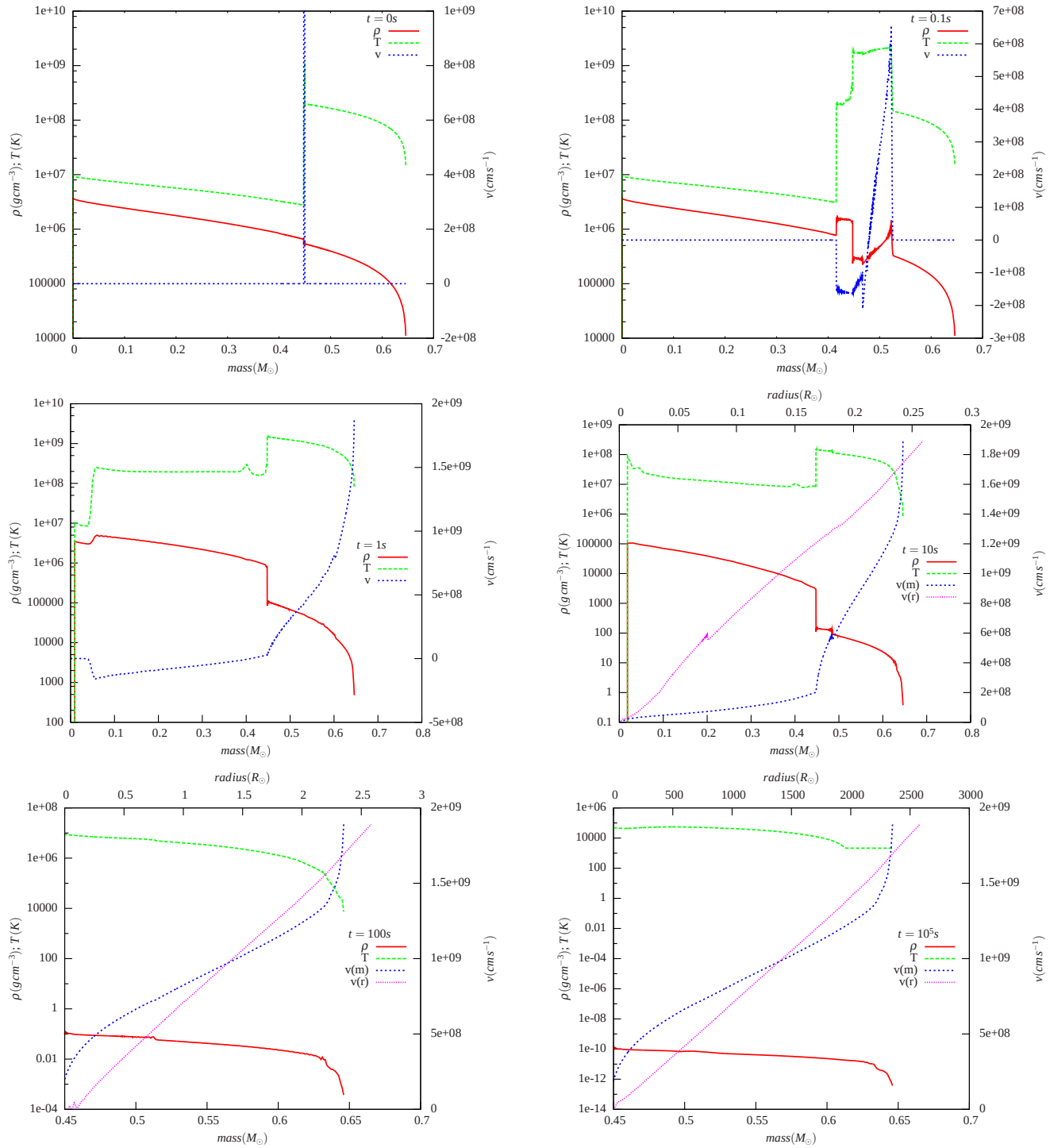

FIG. 1.— Evolution of density (solid red line), temperature (long-dashed green line) and velocity (short-dashed blue line) profile of model CO.45He.2, having a CO core of 0.45 $M_\odot$ and He layer of 0.2 $M_\odot$. From $t = 10$ s, the velocity is homologous, as shown against the radius (dotted purple line).

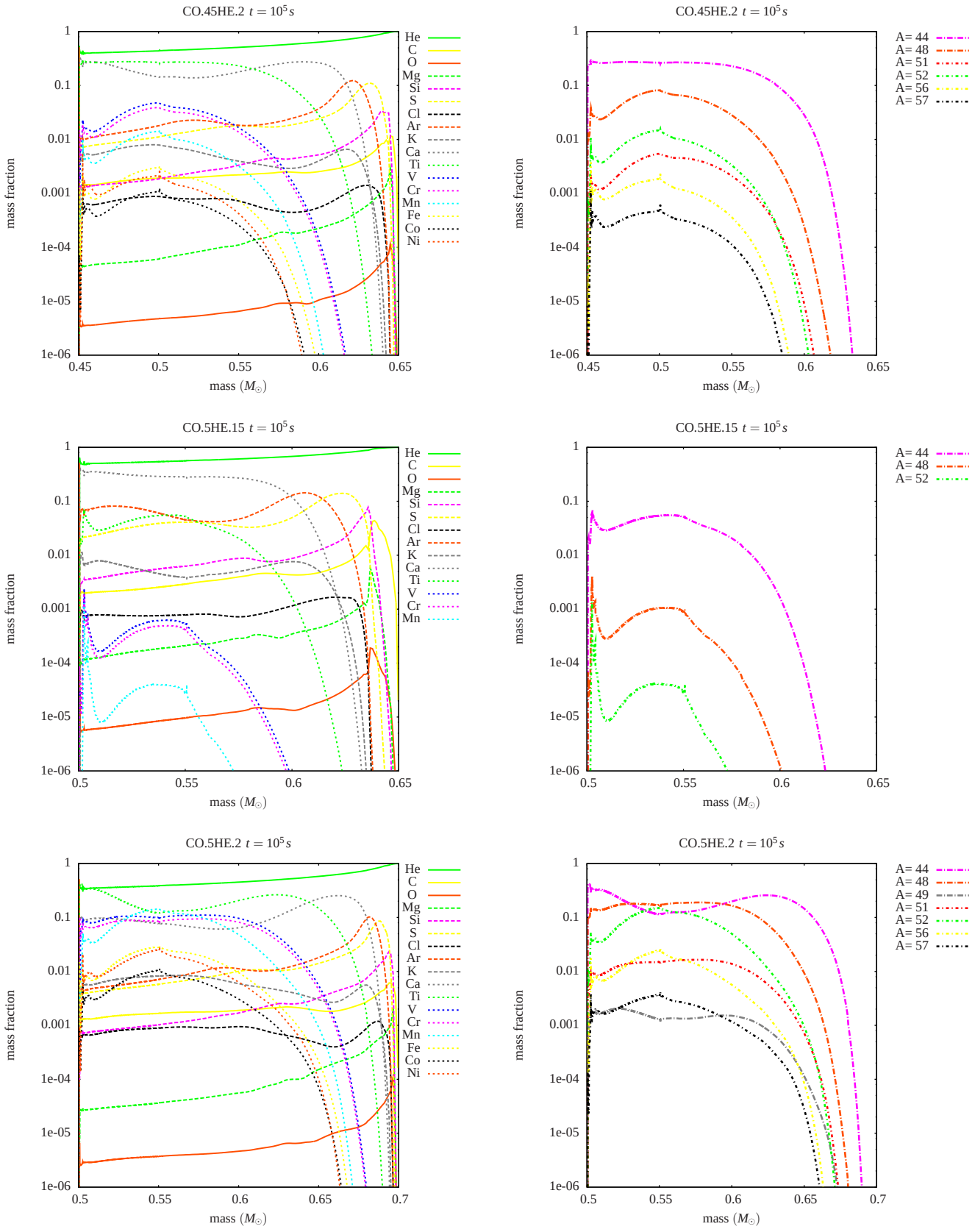

FIG. 2.— The composition profile of our models at epoch $t = 10^5$ s. For each model, the left panel sums up the species by elements; the right panel sums up the nuclei with equal atomic weight (marked on the plot), which form the decay chains followed in the radiative transfer calculations (see Sec. 3). Compositions are showed only if the maximum abundance exceeds 10^{-3}.

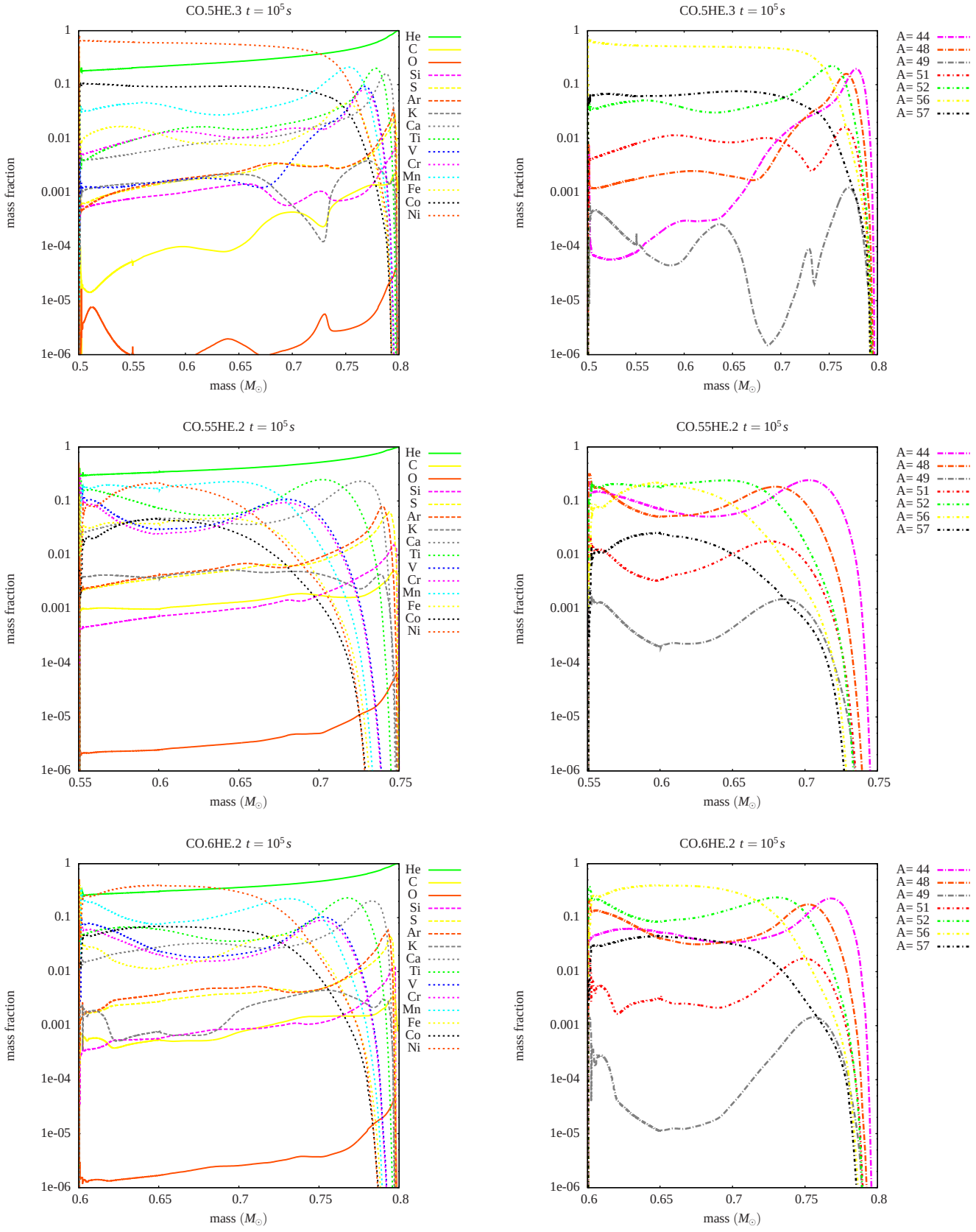

Fig. 2 (continued)

3.1. *Bolometric light curve models*

The code we use to predict UVOIR light curves from the explosion models provides a Monte-Carlo-based, time-dependent description of the propagation of radiative energy packages through the ejecta. The procedure consists of a simulation of the transport of energetic γ-photons released in the radioactive decays within the ejecta and the transport of optical photons generated after the interaction of the γ-photons with the matter. The procedure follows the description given in Cappellaro et al. (1997) and Mazzali et al. (2000).

In addition to the decay of ^{56}Ni as the source of energetic γ-photons we include also a number of other radioactive decay chains that are important to describe the explosion models discussed here. The decays considered are:

$$\begin{aligned}
^{57}\mathrm{Ni} &\rightarrow {}^{57}\mathrm{Co} \rightarrow {}^{57}\mathrm{Fe},\\
^{56}\mathrm{Ni} &\rightarrow {}^{56}\mathrm{Co} \rightarrow {}^{56}\mathrm{Fe},\\
^{52}\mathrm{Fe} &\rightarrow {}^{52}\mathrm{Mn} \rightarrow {}^{52}\mathrm{Cr},\\
^{51}\mathrm{Mn} &\rightarrow {}^{51}\mathrm{Cr} \rightarrow {}^{51}\mathrm{V},\\
^{49}\mathrm{Cr} &\rightarrow {}^{49}\mathrm{V} \rightarrow {}^{49}\mathrm{Ti},\\
^{48}\mathrm{Cr} &\rightarrow {}^{48}\mathrm{V} \rightarrow {}^{48}\mathrm{Ti},\\
^{44}\mathrm{Ti} &\rightarrow {}^{44}\mathrm{Sc} \rightarrow {}^{44}\mathrm{Ca}.
\end{aligned}$$

For the transport of γ-photons we adopt a constant gray opacity $\kappa_\gamma = 0.027\,\mathrm{cm^2\,g^{-1}}$ and assume that once a γ-package encounters an interaction it deposits all its energy on the spot to generate a package of UVOIR-photons (Swartz et al. 1995). The amount and rate of energy deposited in the ejecta is determined following the method of Ambwani & Sutherland (1988) and Lucy (2005). Some of the decays are accompanied by the emission of positrons which are assumed to deposit their kinetic energy in situ.

The propagation of the resulting UVOIR-photons is modeled in a similar Monte Carlo experiment also adopting a gray opacity κ_{uvoir} which is, however, parameterized in terms of the abundance of Fe-group elements in the ejecta as

$$\kappa_{\mathrm{uvoir}} = 0.25 X_{\mathrm{Fe}} + 0.025(1 - X_{\mathrm{Fe}}) \quad [\mathrm{cm^2 g^{-1}}]. \qquad (2)$$

This parametrization accounts for the much larger line opacity added by the complex ions of Fe-group elements compared to lighter elements and has been used in a number of previous studies (e.g., Mazzali et al. 2001; Mazzali & Podsiadlowski 2006; Sim et al. 2007).

A more detailed description of the modeling procedure will be published in an accompanying paper (Sauer et al, in prep.) where we study more generally the properties of the bolometric light curves from all explosion models described in the beginning of this paper. Here we focus on the properties of the model which provides the best fit to the observed light curve of SN 2005E.

3.1.1. *Results*

We computed bolometric light curves for all explosion models in Table 1. Fig. 3 shows the resulting light curves for all models in comparison to the quasi-bolometric light curve points for SN 2005E (black symbols) and SN 2002bj (blue symbols). We derived the bolometric light curve points for SN 2005E from the photometric data published in Perets et al. (2010a) using the procedure developed in Valenti et al. (2008). In addition we made different assumptions to account for the unobserved U and JHK bands indicated by the error bars on the data points of SN 2005E. For the lower limit we took only the observed data from SN 2005E while for the upper limit we added the contribution of the type Ic SN 2007gr (Hunter et al. 2009). The plot symbols correspond to the intermediate light curve obtained from adding the U and JHK contribution of the type Ia SN 2005cf (Pastorello et al. 2007). Also shown is the bolometric light curve of SN 2002bj (Poznanski et al. 2010).

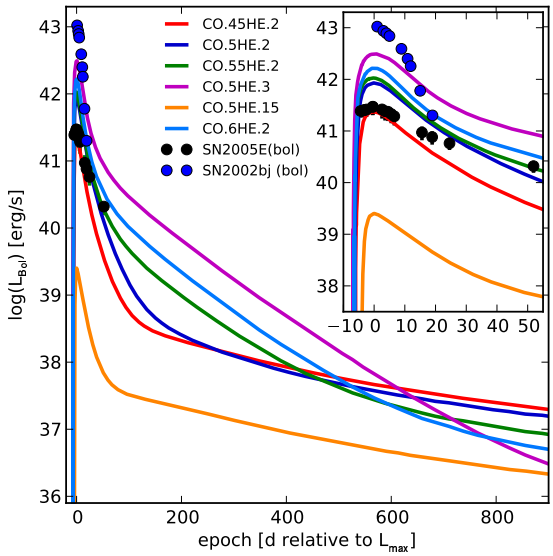

FIG. 3.— Bolometric light curves of all explosion models in comparison to the quasi-bolometric light curve points of the observed supernovae SN 2005E (black circles, Perets et al. 2010a), and SN 2002bj (blue circles, Poznanski et al. 2010). The error bars indicate the range of the bolometric light curve points using different assumptions for unobserved wavelength bands (see text).

All models have a comparable rise time to maximum of about 7 days. Aside from the absolute brightness at maximum light they show strong differences in their late-time behavior. The large range of different light curve properties of those models is primarily due to the variation in the radioactive species synthesized in the explosions which have different energy output and decay timescales. In addition, the models have slightly different density structures resulting from differences in mass and kinetic energy. The latter variation affects the timescales for the diffusion of trapped photons from the ejecta and the brightness at peak. A more in-depth comparison of the different light curve models will be presented in a forthcoming publication. Here we focus merely on the ability of the models to provide a good fit to the observed data of SN 2005E. The best fit to the data points of SN 2005E is provided by the model CO.45HE.2 which has a WD mass of $0.45 M_\odot$ and a He-layer of $0.2 M_\odot$. The model is still somewhat faint at peak and clearly fades more rapidly after maximum light than the observed light curve of SN 2005E. The rise time of the model light curve to maximum light is 6.78 d. Unfortunately the pre-maximum data for SN 2005E is sparse and a good estimate of the rise time is not available; it seems that the rise time in our model is somewhat shorter than the rise time of ∼11 d estimated for SN 2005E (Perets et al. 2010a), but the errorbars on the latter are difficult to es-

timate with the available data. None of our models light curves show similarities with the bright and very fast light curve of SN 2002bj (Poznanski et al. 2010; or the other fast evolving SNe 1885A and 1939B; (Perets et al. 2010c), not shown). The latter bright fast evolving SNe are unlikely to be consistent with the models studied by us.

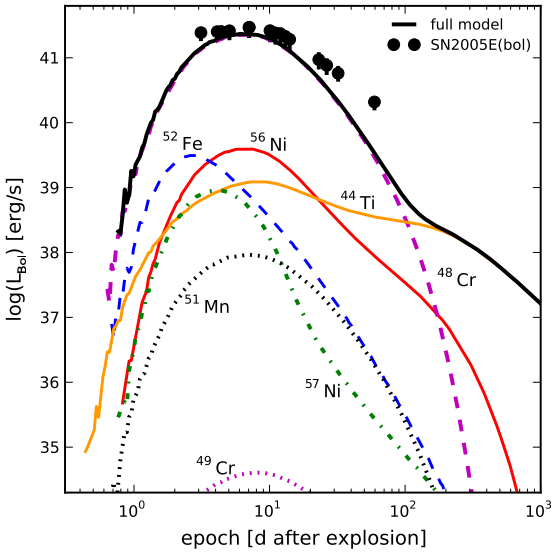

FIG. 4.— Model light curves from the explosion model CO.45He.2 (solid black line) in comparison to the quasi-bolometric light curve of SN 2005E (shifted to the same rise time as the model). The other curves show the contribution of the different radioactive isotopes to the total light curve of this model, each labeled with the first isotope of the respective β^+-decay chain.

Figure 4 shows the light curve of model CO.45HE.2 alone (solid black line) in comparison to the observed data points (shifted to have the same rise time as the model). In addition, the contribution of the different β^+ decay chains to the total light curves are shown, labeled with the first isotope of each chain. In this particular model ^{44}Ti is actually the most abundant radioactive species by mass, however, due to its long half life of 60 years, this decay only dominates the light curve at late times after ∼200 d. The dominant contributor to the light emission around peak is the decay chain ^{48}Cr→^{48}V→^{48}Ti. The time scale of this decay is dominated by the half life of the second decay of 15.97 d. The contribution of the ^{56}Ni/^{56}Co decays, the most important source of radiative energy in normal, radioactively powered supernova light curves, is two orders of magnitude less than the ^{48}Cr/^{48}V contribution in this model.

We also tried to check whether the observed light curve shape can be matched in a better way with slightly different contributions from the various radioactive isotopes. To test this possibility we varied the relative contributions of the different decay chains to the total light curve. In Fig. 5 we show three different models in addition to the original model (solid gray line). In all models the density structure is kept the same, only the relative contributions of the individual light curves shown in Fig. 4 are varied.

Curiously, if one could increase the energy output from the ^{44}Ti decay by a factor of ∼50 this model would provide an excellent fit also to the late-time light curve

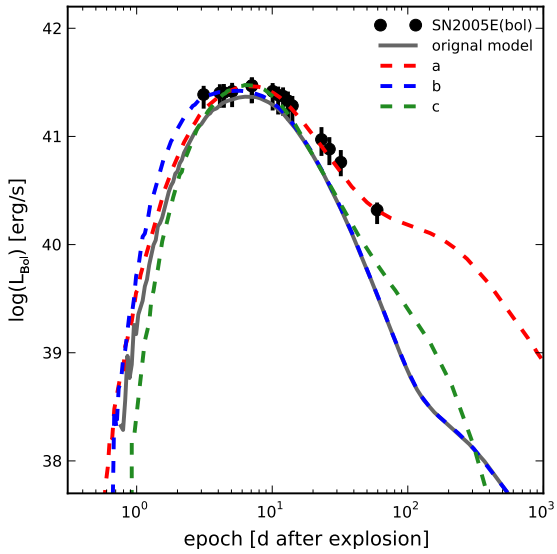

FIG. 5.— Tests if variation of the relative contributions of the radioactive elements can explain the observed shape of the light curve of SN 2005E. In all models only the relative contributions of the individual light curves shown in Fig. 4 are varied. The solid gray line refers to the original model, model *a* was obtained by increasing the ^{44}Ti contribution by a factor of 50. For model *b* ^{52}Fe was enhanced by a factor of 30, model *c* was obtained by only using the ^{56}Ni contribution times a factor of 75 while ignoring all other isotopes.

of SN 2005E (model *a* in Fig. 5). However, because ^{44}Ti is already the most abundant Fe-group element in this model, this increased power cannot be accomplished without changing the mass and density structure of the entire model, which would inevitably lead to a completely different light curve behavior. Nevertheless, this may indicate that the light emission of SN 2005E is dominated by the ^{44}Ti decay already at times shortly after maximum light. A more conclusive assessment would require observations out to much later times of several hundred days after the explosion where one can safely assume that most of the trapped radiation has been released from the ejecta and the short-lived isotopes do not contribute significantly to the light emission anymore.

The pre-maximum data of SN 2005E also indicate that this supernova brightened earlier than the model light curve. A larger contribution of the ^{52}Fe light curve by a factor of ∼30 could explain the early brightening (model *b* in Fig. 5). However, given the sparse data available for SN 2005E a larger ejecta mass leading to a wider light curve cannot be excluded.

Perets et al. (2010a) estimate an ejected mass of $0.275 M_\odot$ and $0.003 M_\odot$ of ^{56}Ni from nebular models of SN 2005E which, however, do not consider any other sources of radiative energy. Model CO.45HE.2 contains $1.1 \times 10^{-4} M_\odot$ of ^{56}Ni. To reproduce the peak of the light curve with ^{56}Ni alone, a factor of ∼ 70 more mass of this isotope (i.e., $\sim 7.8 \times 10^{-3} M_\odot$) is needed (model *c* in Fig. 5). However, with the given density structure ^{56}Ni alone cannot reproduce the decline after maximum. The model light curves decay faster than the observation.

In summary, the decline of the post-maximum light curve of SN 2005E indicates that the ejected mass in SN 2005E might be somewhat larger than proposed by the explosion models. The ^{44}Ti decay in the model can

explain the shape but not the absolute brightness of the late time decline. The pre-maximum light curve also hints towards a larger ejecta mass, some contribution to the early brightening might be explained by the contribution of the ^{52}Fe decay chain.

3.2. *Spectral models*

We used our Monte Carlo spectral synthesis code to derive a sequence of spectral models from the explosion models. The code is based on the description by Mazzali & Lucy (1993); Lucy (1999), and Stehle et al. (2005) and has been successfully used in the past for the efficient interpretation of observed supernova spectra (e.g., Mazzali et al. 2006, 2008; Sauer et al. 2008). The numerical methods are described in more detail in the aforementioned publications, here we discuss only the most important assumptions as far as they are important for the models.

The code computes a stationary solution for the radiative transfer through the supernova ejecta using a Monte Carlo method with an approximate non-LTE description for the atomic level populations. The underlying density structure is taken from the hydrodynamic model for explosion and is expanded homologously according to the time after explosion for each model, assuming that the radiation does not alter the hydrodynamic structure of the explosion. The radius-dependent composition is extracted from the nucleosynthesis results of the explosion model. For radioactive species with appreciable abundance and relevant decay time scales, the conversion to the respective daughter elements is taken into account according to the epoch. Specifically, the decay chains treated explicitly are:

$^{57}\mathrm{Ni} \rightarrow {}^{57}\mathrm{Co} \rightarrow {}^{57}\mathrm{Fe}$,
$^{56}\mathrm{Ni} \rightarrow {}^{56}\mathrm{Co} \rightarrow {}^{56}\mathrm{Fe}$,
$^{52}\mathrm{Fe} \rightarrow {}^{52}\mathrm{Mn} \rightarrow {}^{52}\mathrm{Cr}$,
$^{48}\mathrm{Cr} \rightarrow {}^{48}\mathrm{V} \rightarrow {}^{48}\mathrm{Ti}$.

The solution of the radiative transfer assumes a Schuster-Schwarzschild situation imposing a sharp inner boundary where all radiation is emitted as a blackbody. This implies that the γ-photons and positrons from radioactive decays below this inner boundary are assumed to thermalize, the energy deposition above the inner boundary is not taken into account. In supernova ejecta it is generally difficult to make a clear choice of where to place the inner boundary because the density structure of unbound ejecta tends to be very shallow such that the location where the ejecta become optically thick varies strongly with wavelength (e.g., Sauer et al. 2006). For the models discussed here we chose this location iteratively based on the dilution of the radiation field such that the dilution factor W becomes close to 0.5 (see Mazzali & Lucy 1993 for a discussion of how W is determined in our model). With that choice v_0 corresponds to the location where the radiation field becomes roughly isotropic.

The approximation of stationarity also implies that we cannot determine the luminosity of the model self-consistently because the emitted radiative energy at a given time has contributions from both the directly deposited energy from radioactive decays and the radiation originating from earlier decays which is stored in the optically thick ejecta and diffuses out as the ejecta expand. Therefore, we use the bolometric luminosity at a given epoch from the models of the bolometric light curves discussed in the previous section.

Once the ejecta start to become diluted enough that they are transparent over a wide range of the spectrum, the lower-boundary approximation will fail. For the explosion models discussed here this generally happens already fairly early at about 10 days after maximum because the ejected mass of all models is low. In contrast to the light curve models which do not depend on the photospheric assumption, we cannot compute meaningful spectra beyond the epoch where that approximation breaks down.

Another complication involves the non-thermal excitation of He I. He I has high-lying energy levels such that the ejecta temperatures are too low to populate those levels thermally to give rise to visible absorption lines in the spectrum. The He I absorption features seen in SN Ib (hydrogen-deficient supernovae with visible helium lines, see Filippenko 1997 for a detailed discussion of different types of supernova spectra) are caused by non-thermal excitations from fast electrons which result from Compton-scatterings of the γ-photons released by radioactive decays in the ejecta (e.g. Lucy 1991; Kozma & Fransson 1992; Mazzali & Lucy 1998).

The spectral code we use in this study does not include those non-thermal excitations and ionizations self-consistently. Therefore, the models will not show significant He I absorption features even though the explosion models predict that the He-rich material is well mixed into the zones that have a high abundance of radioactive isotopes. Nevertheless, assuming that the opacity contributed by the relatively few He I lines will not substantially affect the model, the other aspects of the synthetic spectra should predict the observable characteristics of the explosion models reasonably well.

3.2.1. *Results*

Fig. 6 shows a series of synthetic spectra from the explosion model CO.45HE.2 between day 1 and 16 after explosion. The flux of each spectrum in this plot has been normalized with respect to the maximum flux to make the differences in the spectral shape visible. The lower two panels show the two spectra of SN 2005E available during the photospheric phase. The Jan 16 spectrum corresponds to an epoch of $\sim$3 d before maximum light, the Feb 6 spectrum was taken $\sim$18 d after maximum. The input values for the luminosity and the inner boundary velocity v_0 for all spectral models in this series are shown in Fig. 7.

The most prominent ion dominating most of the spectral shape at all times is Ti II. Also visible are the characteristic absorption features from Ca II at $\sim$3900 Å and around 8300 Å. The first spectrum in this series is fairly red because of the low luminosity on day 1. Day 2 shows then a much bluer spectrum which gradually becomes redder as time goes on. All spectra show only very little flux blue of the Ca II absorption at $\sim$3900 Å. In this region the flux is effectively blocked by a dense forest of lines from Fe-group elements, mostly Ti II (cf. Fig 8). Comparing the overall shape of the model spectra to the two observed spectra one notices that the models show most of the observed features, however, the

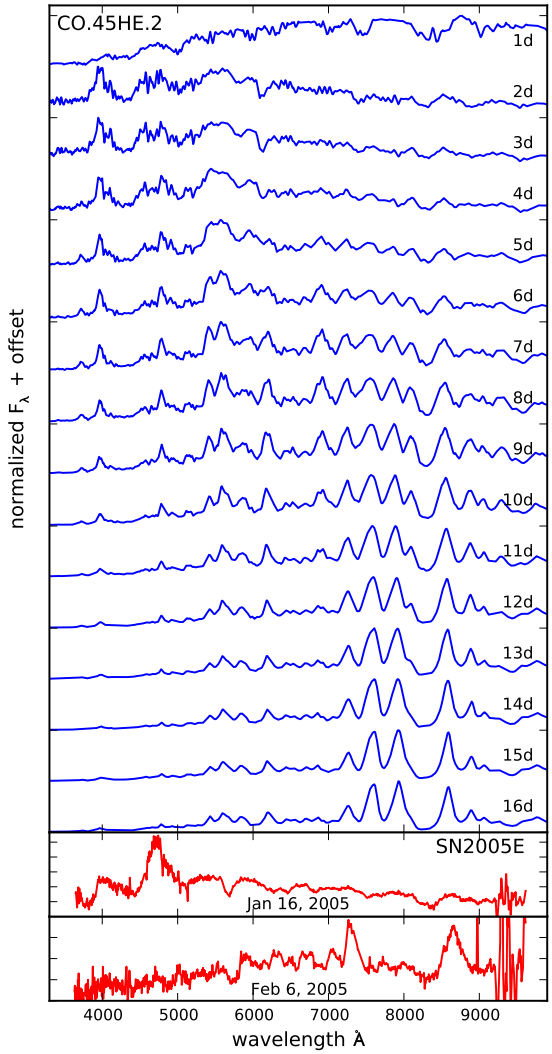

FIG. 6.— Series of synthetic spectra for the explosion model CO.45HE.2 (upper panel). The epoch indicated at each spectrum is given relative to the explosion date. The absolute flux scale has been normalized to the peak of each spectrum to allow for a comparison of the spectral shapes. The (bolometric) maximum of this model occurred 6.78 d after explosion. The lower panels show the observed spectra of SN 2005E ∼3d before and ∼18 d after maximum light.

strength of absorptions and emission peaks are not well reproduced. The spectra before maximum light show a prominent peak at ∼4000 Å which is not as prominent in the observed pre-maximum spectrum. In contrast, the observed spectrum shows a prominent feature at ∼4800 Å which is partially suppressed by absorption features in the model series.

In the post-maximum phases the model spectra evolve faster than the observed spectrum would suggest. This is consistent with the light curve model not reproducing the observed late-time behavior of SN 2005E. Note that the epoch of the Feb 6 spectrum relative to the observed maximum of SN 2005E is later than the relative epoch of the last model spectrum in the series. The model spectra after maximum light show strong re-emission features between 7500 and 9000 Å. Indication for those features are present in the observed spectrum, however at very different relative strengths. The strong features in the

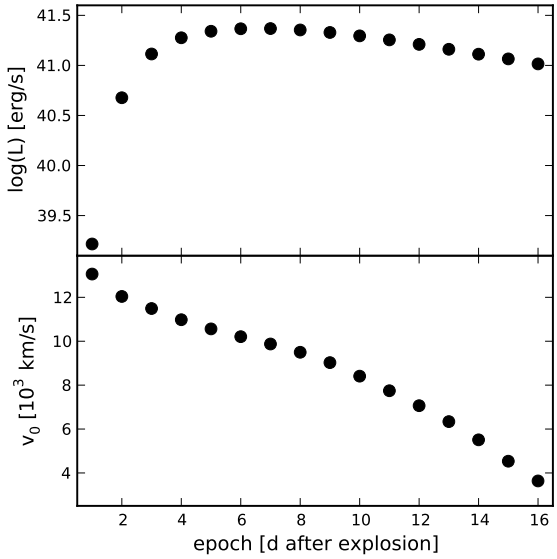

FIG. 7.— Input luminosity (upper panel) and velocity of the inner boundary (lower panel) for the spectral models as a function of time after explosion.

model spectra originate from strong absorptions and the respective re-emission peaks from Ti II lines.

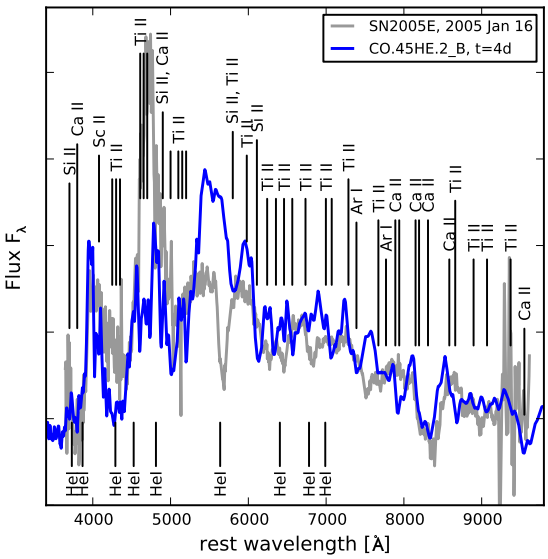

FIG. 8.— Comparison of the synthetic spectrum from the model CO.45He.2 four days after explosion (corresponding to ∼3 days before maximum light) to the observed spectrum of SN 2005E. The flux of the model has been multiplied by a constant to match the observed brightness of SN 2005E at this epoch. The labels above the spectra indicate the ions that form the main contribution to the respective absorption feature. The labels below the spectra indicate the positions where the stronger He I lines are expected in the model spectrum if the model would treat non-thermal excitation of He I (see text).

Fig. 8 shows a detailed comparison of the model spectrum for day 3 and the observed pre-maximum spectrum of SN 2005E. The flux of the model spectrum has been scaled by an arbitrary factor to match the luminosity of the observed spectrum by eye. In this figure the most important ions contributing to observed spectral features are labeled above the spectra. In particular Ti II lines also contribute to most other features in the spectrum.

However, for clarity not all are labeled explicitly. Below the spectra the positions are indicated where one would expect the strongest He I lines to show up if the model included non-thermal excitations of this ion.

The overall shape of the spectrum is reproduced reasonably well by the model. The line velocities and widths are overall correct indicating that the ejecta velocities observed in SN 2005E can be explained by the explosion model. The strong peak at ∼4700 Å seen in the observed spectrum is blocked by a number of strong Ti II lines in the model. Consequently, we see a strong re-emission peak redwards at ∼5500 Å. The model shows Si II lines at 4880, 5800 and 6100 Å, which are not or only very weakly present in the observed spectrum. Especially the absence of the strong Si II 6347, 6371 absorption in the observation indicates that the ejecta of SN 2005E contain only little Si. The total mass of Si in the ejecta of model CO.45HE.2 is $10^{-3} M_\odot$.

In summary, it appears that the composition of the explosion model can reproduce the observed spectrum, perhaps the Ti content is somewhat too high in the model, however the features from intermediate mass elements such as S and Si are also stronger in the model than in the observation. A caveat is that the radioactive isotopes are present in the ejecta at almost all velocities. The effects of non-thermal ionizations and excitations caused by the decays are not accounted for in the radiative transfer model.

4. CONCLUSIONS

Limited to spherical symmetry, we explored the consequences of helium detonations in helium layers accreted on CO cores for a range of core masses. Recent studies by Shen et al. (2010) explored similar scenarios. Their models, however, focused on CO cores of $\geq 0.6\, M_\odot$, while we studied models with CO cores of $\leq 0.6\, M_\odot$, and extended the range of masses to the lowest reasonable limit of $0.45\, M_\odot$. In all cases we assumed that carbon is not ignited. Our study and that of Shen et al. (2010) are therefore complementary. We presented here the scenario of a CO core of $0.6\, M_\odot$ with $0.2\, M_\odot$ of helium layer. This scenario is comparable to the lowest mass cores scenarios explored by Shen et al. (2010). Given the different methods and simulation codes used, our results and those of Shen et al. (2010) are in good agreement, showing quite similar light curves and nucleosynthesis products.

Our results show that below a CO core mass of $0.6\, M_\odot$, the abundance of ^{56}Ni, produced by the detonation, drops rapidly, while those of ^{40}Ca, ^{44}Ti, and ^{48}Cr grow rapidly to a few percent. Moreover, the fraction of unburnt helium also grows with decreasing CO core mass. These findings are encouraging for the discussed scenario to be a viable model for SN 2005E-like objects, and suggest that the latter, low mass CO core scenarios on which we focused are the more likely progenitors of these explosions. It is important to note that, in a narrow mass range of models, a highly diverse outcome is expected, both in terms of light curves and nucleosynthesis. Hence, one cannot expect an accurate fit of a model to a specific observed supernova. Nevertheless, more detailed calculations of the spectra, including the helium lines and late nebular spectra are yet to be done.

Besides the spectrum, the main remaining question concerns the multi dimensional aspect of the problem, which has a strong impact on whether a consecutive CO detonation may follow the helium detonation or not. We speculate that in the 2D case and with low CO core masses ($0.5\, M_\odot$ and under), the density of the core around the possible ignition sites will be too low for CO ignition. The late evolution to thermonuclear runaway and the onset of helium detonation are also issues which require at least two dimensional tools. This is due to the convective nature of the reactive flow at the base of the helium layer, prior to runaway. Dredge up of heavier nuclei into the helium layer could in principle alter the conditions for a transition from quasi-static burning to a detonation.

In terms of nucleosynthetic products, the large abundances of ^{40}Ca and ^{44}Ti produced in our detailed explosion models confirm similar results obtained with the simplified one-zone nucleosynthetic calculation discussed in Perets et al. (2010a). As discussed there, our detailed model results could therefore have important implications for the calcium enrichment of the interstellar medium as well as the the production of positrons and the production of the 511 keV annihilation line.

Finally, if SN 2005E type objects are produced by helium detonations on small CO cores, there should also be a subclass of objects formed by helium detonations on larger cores. In that class the spectrum should be dominated by lines of radioactive nickel, and the probable ignition of the CO core should produce much more energetic and metal rich objects. We therefore encourage observers to search for such supernovae in the near future.

Thanks to Stefano Valenti for computing the quasi-bolometric light curve of SN 2005E from the observed data. We are grateful for Stuart Sim and Markus Kromer at the Max-Planck Institute for Astrophysics for computing a radiative transfer model to cross-check our model results. Nuclear half lives and decay energies used in the light curve model calculations have been compiled using NuDat 2.5 (`http://www.nndc.bnl.gov/nudat2`) and the Web-based Table of Nuclides of the Korea Atomic Energy Research Institute (`http://atom.kaeri.re.kr`). Joint research by A.G. and P.A.M. is supported by a Weizmann-Minerva grant. The work of A.G. is also supported by the Israeli Science Foundation, an EU FP7 Marie Curie IRG fellowship, and a research grant from the Peter and Patricia Gruber Awards. This work is supported in part at the Argonne National Laboratory by the DOE under contract No. DE-AC02-06CH11357, and at the University of Chicago by the NSF under grant PHY 08-22648 for the Physics Frontier Center "Joint Institute for Nuclear Astrophysics" (JINA).

REFERENCES

Ambwani, K., & Sutherland, P. 1988, ApJ, 325, 820
Cappellaro, E. et al. 1997, A&A, 328, 203
Chevalier, R. A., & Plait, P. C. 1988, ApJ, 331, L109
de Vaucouleurs, G., & Corwin, H. G., Jr. 1985, ApJ, 295, 287

Filippenko, A. V. 1997, ARA&A, 35, 309
Fink, M., Hillebrandt, W., Röpke, F. K., 2007, A&A, 476, 1133
Hunter, D. J., et al. 2009, A&A, 508, 371
Kozma, C., & Fransson, C. 1992, ApJ, 390, 602
Livne, E., 1990, ApJLet., 354L, 53
Livne, E.& Glasner,A.,S., 1990, ApJ, 361, 244
Livne, E.& Glasner,A.,S., 1991, ApJ, 370, 272
Livne, E., & Arnett,D., 1995, ApJ, 452, 62
Lucy, L. B. 1991, ApJ, 383, 308
—. 1999, A&A, 345, 211
—. 2005, A&A, 429, 19
Mazzali, P. A., Iwamoto, K., & Nomoto, K. 2000, ApJ, 545, 407
Mazzali, P. A., & Lucy, L. B. 1993, A&A, 279, 447
—. 1998, MNRAS, 295, 428
Mazzali, P. A. et al. 2001, ApJ, 547, 988
Mazzali, P. A., & Podsiadlowski, P. 2006, MNRAS, L32
Mazzali, P. A. et al. 2008, MNRAS, 386, 1897
Mazzali, P. A., et al. 2006, Nature, 442, 1018
Nomoto, K., 1980, Proc. Texas Workshop on Type Ia Supernovae, ed. J. C. Wheeler, (Austin: Univ. Texas Press), 164
Nomoto, K., 1982, ApJ, 257, 780
Pastorello, A., et al. 2007, MNRAS, 376, 1301
Perets, H. B., et al. 2010a, Nature, 465, 322
Perets, H. B., et al. 2010b, in preparation
Perets, H. B., et al. 2010c, arXiv:1008.275
Poznanski, D., et al. 2010, Science, 327, 58
Sauer, D. N., Hoffmann, T. L., & Pauldrach, A. W. A. 2006, A&A, 459, 229
Sauer, D. N., et al. 2008, MNRAS, 391, 1605
Shen, K. J., & Bildsten,L., 2009, ApJ, 699, 136
Shen, K. J., Kasen, D., Weinberg, N. N., Bildsten, L., & Scannapieco, E., 2010, ApJ, 715, 767
Sim, S. A. et al. 2007, MNRAS, 378, 2
Stehle, M. et al. 2005, MNRAS, 360, 1231
Swartz, D. A., Sutherland, P. G., & Harkness, R. P. 1995, ApJ, 446, 766
Valenti, S., et al. 2008, MNRAS, 383, 1485
Weiss, A., & Truran, J. W., 1990, A&A, 238, 178
Woosley, S. E., Weaver, T. A. & Taam, R. E., 1980, Proc. Texas Workshop on Type Ia Supernovae, ed. J. C. Wheeler, (Austin: Univ. Texas Press), 96
Woosley, S. E., Taam, R. E. & Weaver, T. A., 1986, ApJ, 301, 601
Woosley, S. E., & Weaver, T. A., 1994, ApJ, 423, 371
Yoon, S. C. & Langer, N., 2004, A&A,419, 645

TABLE 1
PARAMETERS OF THE SIMULATED INITIAL CONFIGURATIONS

Model	M_{CO}	M_{He}	ρ_{6c}	T_{7c}	ρ_{6He}	T_{7He}
CO.45HE.2	0.45	0.2	3.81	1.	0.543	20.
CO.5HE.15	0.5	0.15	3.92	1.	0.402	20.
CO.5HE.2	0.5	0.2	5.06	1.	0.678	20.
CO.5HE.3	0.5	0.3	8.50	1.	1.391	20.
CO.55HE.2	0.55	0.2	6.72	1.	0.845	20.
CO.6HE.2	0.6	0.2	8.81	1.	1.032	20.

NOTE. — mass units=$M_{\odot}$, ρ_{6c} is the central density in units of $10^6 g\, cm^{-3}$, ρ_{6He} is the density at the base of the helium shell in same units, T_{7c} and T_{7He} are the corresponding temperatures in units of $10^7 K$.

TABLE 2
Explosion Energy and Nucleosynthesis Products

Isotope	CO.45HE.2	CO.5HE.15	CO.5HE.2	CO.5HE.3	CO.55HE.2	CO.6HE.2
Ek	0.178	0.096	0.201	0.460	0.226	0.242
^{4}He	1.1E-01	9.8E-02	1.0E-01	9.7E-02	9.3E-02	8.3E-02
^{20}Ne	9.8E-06	1.2E-05	6.5E-06	3.9E-06	4.7E-06	3.7E-06
^{23}Na	1.2E-09	2.0E-09	6.0E-10	1.4E-09	3.0E-10	1.6E-10
^{24}Mg	4.4E-05	6.2E-05	2.7E-05	1.3E-05	1.8E-05	1.4E-05
^{27}Al	9.9E-07	1.1E-06	7.0E-07	3.1E-07	4.5E-07	4.0E-07
^{28}Si	1.0E-03	1.5E-03	5.8E-04	1.7E-04	3.8E-04	2.7E-04
^{31}P	1.8E-05	2.2E-05	1.2E-05	2.6E-05	8.3E-06	6.6E-06
^{32}S	4.6E-03	6.9E-03	2.7E-03	5.5E-04	1.7E-03	1.1E-03
^{35}Cl	1.4E-04	1.3E-04	1.5E-04	1.3E-04	1.2E-04	6.6E-05
^{36}Ar	5.5E-03	9.1E-03	3.2E-03	6.0E-04	1.9E-03	1.4E-03
^{39}K	9.4E-04	6.8E-04	1.1E-03	4.9E-04	8.2E-04	4.1E-04
^{40}Ca	3.4E-02	2.9E-02	2.1E-02	5.5E-03	1.3E-02	9.0E-03
^{41}Ca	3.3E-06	1.8E-06	5.4E-06	1.3E-06	4.9E-06	2.3E-06
^{42}Ca	5.3E-06	1.1E-06	1.8E-05	8.3E-06	1.5E-05	4.7E-06
^{43}Ca	8.4E-05	2.3E-05	1.1E-04	5.3E-05	8.0E-05	5.3E-05
^{44}Ca	1.4E-06	1.7E-07	1.3E-06	2.3E-07	7.9E-07	5.2E-07
^{45}Sc	1.6E-05	1.8E-06	1.5E-05	2.1E-06	8.2E-06	3.8E-06
^{44}Ti	3.3E-02	3.2E-03	3.1E-02	5.8E-03	2.0E-02	1.3E-02
^{46}Ti	4.0E-06	5.8E-07	4.2E-06	7.8E-04	2.8E-06	6.9E-05
^{47}Ti	3.7E-04	1.8E-05	7.4E-04	1.8E-03	6.0E-04	4.6E-04
^{48}Ti	9.4E-05	8.0E-07	3.5E-04	8.8E-05	2.7E-04	2.2E-04
^{49}Ti	1.4E-07	1.5E-09	4.6E-07	1.3E-07	2.6E-07	1.2E-07
^{47}V	1.1E-06	2.0E-08	5.2E-06	6.1E-08	9.2E-06	2.9E-06
^{48}V	3.2E-03	2.7E-05	1.2E-02	3.0E-03	9.4E-03	7.4E-03
^{49}V	6.0E-05	6.2E-07	2.0E-04	5.5E-05	1.1E-04	5.2E-05
^{51}V	1.0E-05	5.9E-08	4.7E-05	6.5E-05	3.9E-05	2.7E-05
^{48}Cr	2.3E-03	2.0E-05	8.7E-03	2.2E-03	7.0E-03	5.5E-03
^{49}Cr	1.4E-07	4.4E-10	7.7E-07	3.1E-08	2.2E-06	1.4E-06
^{50}Cr	2.0E-05	2.3E-07	6.1E-05	3.8E-04	3.6E-05	3.2E-05
^{51}Cr	3.6E-04	2.1E-06	1.7E-03	2.3E-03	1.4E-03	9.4E-04
^{51}Mn	2.4E-07	2.2E-10	2.5E-06	2.3E-07	1.6E-05	1.4E-05
^{52}Mn	7.8E-04	2.0E-06	9.1E-03	1.6E-02	2.4E-02	2.1E-02
^{53}Mn	5.0E-05	1.2E-07	5.7E-04	2.6E-04	1.2E-03	4.7E-04
^{51}Fe	9.7E-08	4.0E-11	7.9E-07	2.2E-07	2.5E-06	2.3E-06
^{52}Fe	8.5E-05	2.1E-07	9.9E-04	1.7E-03	2.7E-03	2.6E-03
^{53}Fe	2.6E-08	2.9E-12	3.3E-07	7.7E-09	5.7E-06	1.6E-05
^{54}Fe	1.7E-05	4.2E-08	1.5E-04	3.7E-04	2.7E-04	1.2E-04
^{55}Fe	7.8E-05	1.2E-07	7.7E-04	1.8E-03	2.4E-03	1.5E-03
^{56}Fe	9.5E-08	1.0E-10	1.0E-06	7.9E-05	1.1E-05	2.7E-05
^{57}Fe	2.2E-08	2.8E-11	1.7E-07	1.0E-05	1.4E-06	3.1E-06
^{55}Co	3.9E-05	5.8E-08	3.8E-04	9.1E-04	1.2E-03	7.8E-04
^{56}Co	1.5E-05	1.5E-08	1.8E-04	1.5E-02	2.0E-03	5.2E-03
^{57}Co	1.3E-05	1.7E-08	1.1E-04	6.4E-03	8.3E-04	2.0E-03
^{56}Ni	9.9E-05	9.8E-08	1.2E-03	1.1E-01	1.4E-02	3.7E-02
^{57}Ni	1.8E-05	2.3E-08	1.5E-04	9.1E-03	1.2E-03	2.8E-03
^{58}Ni	1.6E-05	3.0E-08	1.4E-04	1.8E-02	8.7E-04	2.1E-03
^{59}Ni	1.4E-07	4.4E-10	1.8E-06	3.4E-05	8.6E-06	1.8E-05
^{60}Ni	4.0E-09	2.1E-11	7.7E-08	6.0E-07	4.6E-07	1.0E-06

Note. — The products listed include the He layer only, and are given at the beginning of radiative transfer calculation ($t = 10^5 s$). Between He and K, only the most abundant isotope is included, from Ca and up all isotopes exceeding $10^{-6} M_\odot$ in at least one model are listed. EK - final kinetic energy in units of 10^{51} ergs, isotopes - in solar mass.

TABLE 3
End product as a function of initial ^{12}C mass fraction

$X_C(initial)$	N	End-product(^{12}C + Nα)
0.6	2	^{20}Ne
0.5	3	^{24}Mg
0.429	4	^{28}Si
0.375	5	^{32}S
0.33	6	^{36}Ar
0.30	7	^{40}Ca
0.273	8	^{44}Ti
0.25	9	^{48}Cr
0.231	10	^{52}Fe
0.214	11	^{56}Ni